



Contents lists available at ScienceDirect

Journal of Quantitative Spectroscopy & Radiative Transfer

journal homepage: www.elsevier.com/locate/jqsrt

Transmittance of transparent horizontal and tilted windows supporting large non-absorbing pendant droplets



Jack Hoeniges^a, Keyong Zhu^b, William Welch^a, Eylul Simsek^a, Laurent Pilon^{a,*}

^aMechanical and Aerospace Engineering Department, Henry Samueli School of Engineering and Applied Science, University of California, Los Angeles, 420 Westwood Plaza, Los Angeles, CA 90095, USA

^bSchool of Aeronautical Science and Engineering, Beihang University, No. 37, Xueyuan Road, Beijing 100191, China

ARTICLE INFO

Article history:

Received 6 June 2021

Revised 7 August 2021

Accepted 8 August 2021

Available online 12 August 2021

Keywords:

Solar energy

Dropwise condensation

Solar desalination

ABSTRACT

This study establishes that the deviation of large pendant droplets from an ideal cap-shape due to gravity can have significant and complex impacts on the normal-hemispherical and directional-hemispherical transmittances of light through horizontal and tilted transparent windows. First, the shape of pendant droplets larger than the capillary length was predicted numerically by balancing gravitational and surface tension forces for various droplet volumes, contact angles, and window tilt angles. Then, light transfer through windows supporting such numerically generated droplets was simulated using the Monte Carlo ray-tracing method. The window transmittance for large droplets was found to be nearly independent of droplet spatial arrangement and size distribution for relatively narrow size distributions. Furthermore, the droplets could be assumed to be cap-shaped in predicting the normal-hemispherical transmittance for droplet volumes $V < 10 \mu\text{L}$ and contact angles $\theta_c < \theta_{cr}$ where θ_{cr} is the critical angle for total internal reflection at the droplet/air interface. However, for larger droplets and/or contact angles, assuming droplets to be cap-shaped caused the transmittance to be overestimated by as much as 37% for horizontal windows. This was due to gravity-induced deformation of the droplet shape resulting in increased reflection at the droplet/air interface. For tilted windows, the droplet deformation caused the normal-hemispherical transmittance to increase with increasing droplet volume and window tilt angle. For both horizontal and tilted windows, transmittance decreased linearly with increasing droplet surface area coverage. These results and numerical tools can be used to design energy efficient solar stills, greenhouses, and covered photobioreactors, for example.

© 2021 Elsevier Ltd. All rights reserved.

1. Introduction

In many solar energy conversion applications such as solar stills, greenhouses, and microalgae cultivation systems, direct exposure to sunlight increases the temperature of the system and drives water evaporation, thus increasing the relative humidity within the system [1]. Then, condensate droplets form on the interior surface of the windows or cladding if their temperature falls below the dew point of the interior air due to emission of infrared radiation to the sky and exposure to colder outside air and wind. For example, Fig. 1a depicts a solar still under operation wherein salt water is heated by the incident solar radiation resulting in evaporation and water droplets condensing on the inner surface of the tilted window cover to produce fresh water. Similarly, Fig. 1b shows a greenhouse used to cultivate plants year-round with con-

densation present on its inner windows. Finally, Fig. 1c pictures a covered raceway pond used for green microalgae cultivation with droplets condensing on the inner surface of the transparent cover [2].

The presence of droplets on transparent windows has been shown to decrease their transmittance in the visible part of the electromagnetic spectrum [3–8]. The reduction in the amount of energy entering the system limits the productivity of greenhouses and microalgae cultivation systems as they both rely on visible light to drive photosynthesis [2,6]. Furthermore, droplet shape has been shown to play an important role in the productivity of solar stills [9]. The use of hydrophobic windows with larger droplet contact angles was found to reduce solar still productivity by approximately 45% due to the decrease in the window transmittance compared to windows with smaller droplet contact angles [9]. Previous theoretical studies [3,7,8,10–13] considered small cap-shaped droplets whose shape was dominated by surface tension forces and featured a constant radius of curvature. This assumption is valid provided that the droplet size is much smaller than the capillary

* Corresponding author.

E-mail address: pilon@seas.ucla.edu (L. Pilon).

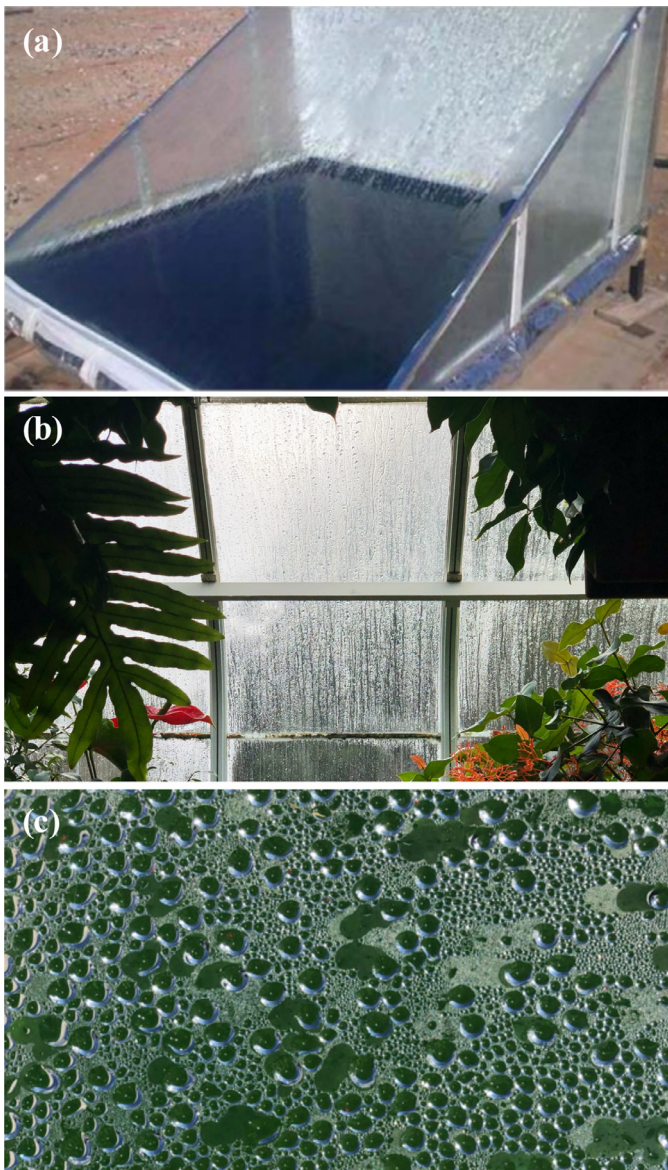


Fig. 1. Examples of condensation in enclosed systems including (a) a solar still (photo used with permission of V-EnerTek, Chennai, India. All rights reserved. ©2021 V-EnerTek), (b) the interior of a greenhouse (image credit: <http://www.finestgreenhouse.com>), and (c) a covered raceway pond for microalgae cultivation at the R&D facility AlgoSolis (Saint-Nazaire, France).

length l_c defined as [14]

$$l_c = \sqrt{\frac{\sigma}{\rho g}} \quad (1)$$

where σ is the surface tension of the droplet/air interface, ρ is the droplet density, and g is the gravitational acceleration. For water droplets in air, the capillary length is $l_c = 2.7$ mm. In the case of the solar stills, greenhouses, and covered microalgae raceway ponds illustrated in Fig. 1, condensation occurs over the course of hours, enabling droplets to attain sizes on the same order or larger than the capillary length l_c . Then, droplets cannot be assumed to be cap-shaped as gravity can significantly affect their shape [14]. To the best of our knowledge, the effect of such large non-cap shaped pendant droplets on the transmittance of both horizontal and tilted windows has not been investigated to date.

This study aims to quantify the impact of the shape of large and non-absorbing pendant droplets on the transmittance of hori-

zontal and tilted transparent windows. To do so, the droplet shape was predicted numerically by balancing gravitational and surface tension energies. Then, the normal-hemispherical and directional-hemispherical transmittances of the windows were predicted numerically for a wide variety of droplet configurations. The results were compared with those obtained for cap-shaped droplets with the same volume and contact angle.

2. Background

Briscoe and Gavin [3] theoretically investigated the normal-hemispherical transmittance, at wavelength of 650 nm, of a 1.1 mm thick transparent window ($n_w = 1.5$) supporting a single small cap-shaped droplet ($n_d = 1.33$). To do so, a ray-tracing analysis was performed for 200 rays evenly distributed along the radial direction of the droplet and incident on the dry side of the window. The window and droplets were assumed to have the same absorption coefficient $\kappa_w = \kappa_d = 0.04 \text{ mm}^{-1}$. For a projected droplet diameter of 50 μm , the transmittance through the droplet was found to be essentially unchanged for contact angles $\theta_c \leq 40^\circ$ and to decrease from approximately 90% to as low as 50% as the contact angle θ_c increased from 40° to 90° . The decrease was attributed to an increase in total internal reflection at the droplet/air interface for droplet contact angle $\theta_c > \theta_{cr}$ where the critical angle θ_{cr} is given by $\theta_{cr} = \sin^{-1}(n_d/n_w) = 48.6^\circ$. For cap-shaped droplets, the droplet shape was self-similar over the range of projected diameters investigated for a given contact angle. Thus, the transmittance was found to be independent of droplet projected diameter for the optical properties considered and was instead controlled by the droplet shape via the contact angle.

Pieters et al. [15] developed an experimental method to record the temporal evolution of the shape of an evaporating water droplet on a vertical polyethylene film. The contact angle of water droplets on polyethylene is approximately 100° [3]. The resulting 3D contours were used to theoretically predict the directional-hemispherical transmittance of a single drying droplet on a polyethylene film. The dry area around the droplet was not accounted for in the simulations, i.e., droplet surface area coverage was 100%. The results indicated an increase in the directional-hemispherical transmittance as the droplet evaporated. The authors attributed this observation to the decrease in curvature in the droplet profile as evaporation proceeded. Furthermore, the authors demonstrated that the directional-hemispherical transmittance of the experimentally measured non-cap shaped droplets on a vertical film deviated significantly from that of cap-shaped droplets with a contact angle of 90° , considered to be similar to that of water on polyethylene.

In a later study, Pieters et al. [10] experimentally and theoretically investigated the directional-hemispherical transmittance of light at 632.8 nm through vertical glass ($n_w = 1.526$, $\kappa_w = 4 \mu\text{m}^{-1}$) or polyethylene ($n_w = 1.515$, $\kappa_w = 165 \mu\text{m}^{-1}$) windows with condensate water droplets ($n_d = 1.333$, $\kappa_d = 0.4 \mu\text{m}^{-1}$) on their back side. The authors also simulated the directional-hemispherical transmittance of a single cap-shaped droplet with projected diameter as large as 12.75 mm. Here also, the normal-hemispherical transmittance was found to be independent of the droplet size and to decrease with increasing contact angle θ_c larger than 40° .

Pollet and Pieters [4,5,16] conducted an experimental investigation of light at wavelength 632.8 nm through greenhouse cladding materials including glass and standard, anti-drop-condensation, and anti-dust polyethylene films. The transmittance measurements of a vertically oriented glass window and standard polyethylene film were taken under laboratory conditions for a complete condensation cycle progressing from a dry window, to condensation without droplet run-off, to condensation with droplet run-off, to

the evaporation phase. In the presence of condensation, materials with smaller droplet contact angle (e.g., glass) were found to have transmittance up to 30% larger than those with larger contact angles (e.g., standard and anti-dust-polyethylene films).

Tow [13] theoretically investigated the antireflective potential of droplets on the back side of a glass window using the Monte Carlo ray-tracing (MCRT) method. The directional-hemispherical transmittance was predicted at wavelength 500 nm for a 3 mm thick non-absorbing glass window ($n_w = 1.5$) supporting monodisperse, ordered, and weakly absorbing droplets ($n_d = 1.33$, $\kappa_d = 2.5 \times 10^{-7} \mu\text{m}$). The author considered a window with a single droplet and periodic boundary conditions to simulate an infinitely large droplet-covered window. The droplet was assumed to be cap-shaped with a projected diameter equal to 2.7 mm and contact angle θ_c varying from 6° to 90° . The droplet surface area coverage ranged from 14% to 90%. The presence of droplets was found to slightly increase the normal-hemispherical transmittance compared to a dry window for contact angles θ_c less than the critical angle θ_{cr} . However, the transmittance was found to decrease with increasing contact angle for $\theta_c \geq \theta_{cr}$.

Recently, we have systematically investigated the impact of non-absorbing and absorbing cap-shaped droplets on the normal-hemispherical [7,8,11], the directional-hemispherical [7,8,11], and the bidirectional transmittance [12] of horizontal windows supporting droplets on either their front or back side using the Monte Carlo ray-tracing method in the geometric optics limit. Unlike previous theoretical studies, a wide range of droplet diameter, contact angle, absorption index, and surface area coverage was considered. In addition, simulations were performed for a large number of monodisperse or polydisperse droplets arranged on the window in either a random or ordered hexagonal pattern [7]. The spectral absorptance and transmittance of an absorbing window and droplets for wavelengths from 0.4 to 5 μm were also predicted [8]. In all cases, the droplets were assumed to be small and cap-shaped. The dependence of transmittance on contact angle was found to have four distinct regimes for non-absorbing droplets with contact angle ranging from 10° to 180° [7]. The presence of droplets on the back side of a window was found to decrease its transmittance for droplet contact angles $\theta_{cr} < \theta_c < 180^\circ - \theta_{cr}$ [7]. Furthermore, the different transmittances were found to be independent of droplet size, size distribution, or droplet arrangement provided that droplets were non-absorbing [7,11,12].

Simsek et al. [17], experimentally validated these results in the visible part of the spectrum for $\theta_c < 90^\circ$ both quantitatively and qualitatively. Indeed, the normal-hemispherical transmittance and reflectance of glass windows supporting acrylic droplets was measured in the visible to near-infrared parts of the electromagnetic spectrum (0.4–1.1 μm). Various surface treatments were applied to achieve contact angles between 26° and 76° . The diameter and location of all the acrylic droplets on selected samples were characterized and used as input parameters into the MCRT algorithm to predict their normal-hemispherical transmittance and reflectance. Very good agreement was found between the theoretical predictions and experimental results.

This paper aims to expand on previous studies to investigate the effect of large and non-absorbing droplets on the transmittance of horizontal and tilted droplet-covered windows. First, the droplet shape was found numerically by using energy minimization principles to balance gravitational and surface tension energies. Then, the normal-hemispherical and directional-hemispherical transmittances of the windows were predicted by the Monte Carlo ray-tracing method accounting for reflection and refraction at all interfaces. The impact of droplet (i) spatial arrangement, (ii) size distribution, (iii) volume, (iv) contact angle, (v) window tilt angle, and (vi) surface area coverage were systematically investigated.

3. Analysis

3.1. Problem statement

Let us consider a transparent window supporting large pendant droplets exposed to collimated radiation. The window was non-absorbing with thickness $H = 3$ mm, refractive index $n_w = 1.5$, and was positioned horizontally (Fig. 2a) or tilted at an angle α with respect to the horizon (Fig. 2b). The direction of the incident solar radiation was denoted by the polar θ_i and azimuthal γ_i angles of incidence defined with respect to the positive z-axis and the positive x-axis, respectively. The shape of the droplet/air interface was defined by the radial coordinate $r_d(\psi, \phi)$ where the polar ψ and azimuthal ϕ angles are defined with respect to the negative z-axis and positive x-axis, respectively. The water droplet density ρ was taken as 1000 kg/m^3 and the surface tension σ of the air/droplet interface was 72.1 mN/m . Droplets on horizontal windows had a circular contact line with radius $R_c = r_d(\psi = \pi/2, \phi)$ and projected radius R_p while droplets on the tilted window had a non-circular contact line, as illustrated in Figs. 2c and 2d, respectively. The droplets were non-absorbing and had refractive index $n_d = 1.33$ and arbitrary volume V . The contact angle and the projected surface area coverage of the droplets on the window were denoted by θ_c and f_A , respectively. Droplets were either monodisperse or polydisperse with an arbitrary volume distribution. They were either randomly distributed on the window surface or arranged in an ordered hexagonal pattern. The incident photons underwent reflection or refraction at each interface and were either back-scattered or transmitted through the droplet-covered window.

3.2. Assumptions

The droplet shape was predicted based on the assumptions that the droplets were stationary and had constant volume, density, surface tension, and contact angle. Droplets were only subjected to gravitational and surface tension forces.

The simulations of light transfer through the droplet-covered window were performed using the Monte Carlo ray-tracing method based on the following assumptions: (1) the droplet and window dimensions were much larger than the wavelength of the impinging radiation such that geometric optics was valid. (2) All interfaces were considered optically smooth so that specular reflection and refraction were governed by Snell's law and Fresnel's equations. (3) Both the window and the droplets were non-absorbing.

3.3. Method of solutions

Droplet shape

The droplet shape was determined using the open source *Surface Evolver* program [18]. This program approximates the droplet surface as an ensemble of vertices, edges, and triangular facets. It employs a gradient descent optimization algorithm to iteratively refine and adjust the droplet shape defined by the radial coordinate $r_d(\psi, \phi)$ so as to minimize the sum of its potential and surface energies for a given density ρ and air/droplet surface tension σ while maintaining an arbitrary constant volume V and contact angle θ_c [18]. On tilted windows, the droplet shape also depended on the window tilt angle α and the associated advancing θ_{adv} and receding θ_{rec} droplet contact angles (Fig. 2b). Then, the droplet contact angle varied along the contact line as a function of the azimuthal angle ϕ according to [19,20]

$$\theta_c(\phi) = 2 \left(\frac{\theta_{adv} - \theta_{rec}}{\pi^3} \right) \phi^3 - 3 \left(\frac{\theta_{adv} - \theta_{rec}}{\pi^2} \right) \phi^2 + \theta_{adv}. \quad (2)$$

The resulting droplet contour was output in the form of a triangulation matrix for both horizontal and tilted windows. The tri-

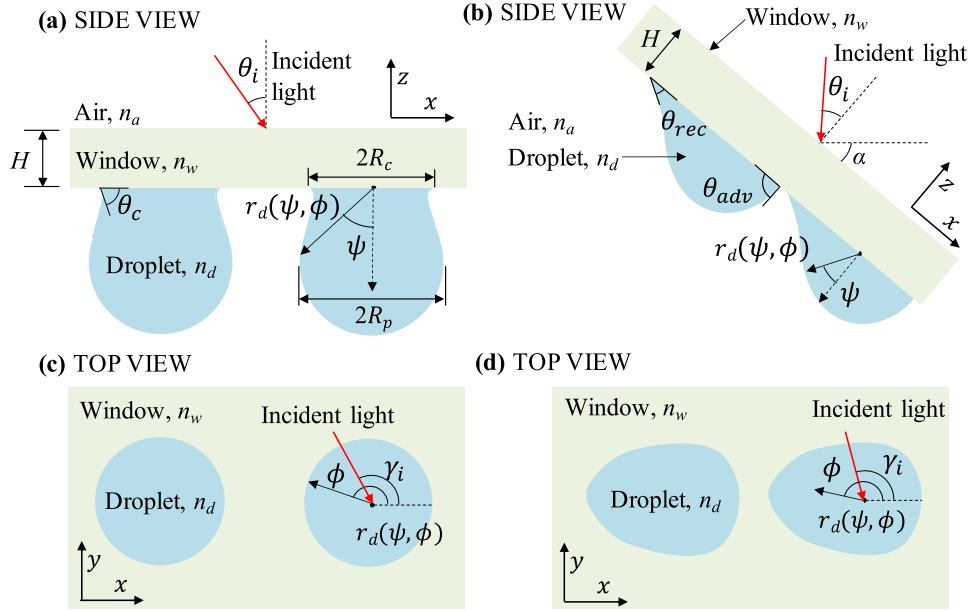


Fig. 2. Side view and top view (not to scale) of (a,c) a horizontal window and (b,d) a tilted window supporting large non-cap shaped pendant droplets featuring the droplet/window contact area.

angulation matrix was then used as an input to the light transfer simulations to determine the location of the droplet/air interface and calculate the incidence angle of the photons.

Light transfer

Light transfer through droplet-covered windows was simulated using the Monte Carlo ray-tracing method. The method and algorithm were explained in detail in Refs. [7,8,11,12] and validated against experimental results in Refs. [7,17] and need not be repeated. In brief, a large number of collimated photon bundles or “rays” were launched normally onto a window supporting pendant droplets generated by the *Surface Evolver* program [18]. At each interface a ray encountered (e.g., air/window, window/droplet, droplet/air interface), the angle of refraction and the reflectivity were determined from Snell’s law and Fresnel’s equations, respectively. Then, a random number from the uniform distribution was generated and compared to the calculated reflectivity to determine if the ray was reflected or refracted. The ray was then either specularly reflected or refracted. Next, the ray was traced to the location of the next interface in the 3D simulation domain. The boundary conditions on the side of the computational domain were periodic. In the case of a non-absorbing window and droplets, this process continued until a ray was either (i) back-scattered by or (ii) transmitted through the droplet-covered window. The normal-hemispherical transmittance T_{nh} corresponded to the fraction of normally incident photons transmitted through the droplet-covered window in any direction, and was computed according to [7]

$$T_{nh}(n_d, V, \theta_c, n_w, \alpha, f_A) = \frac{N_t}{N_i} \tag{3}$$

where N_t is the number of transmitted photons and N_i is the total number of photons incident on the window. Similarly, the directional-hemispherical transmittance T_{dh} was expressed as

$$T_{dh}(n_d, V, \theta_c, n_w, \alpha, f_A, \theta_i, \gamma_i) = \frac{N_t}{N_i} \tag{4}$$

In order to achieve numerical convergence, $N_i = 10^6$ rays were used for each simulation.

4. Results and discussion

4.1. Droplet shape and maximum volume

Fig. 3a shows a photograph of a pendant water droplet of volume $V = 50 \mu\text{L}$ on a PVC slab with tilt angle $\alpha = 24^\circ$ and contact angle $\theta_c = 86^\circ$ when the slab substrate was horizontal (i.e., $\alpha = 0^\circ$). Such a photograph was used to measure the advancing θ_{adv} and receding θ_{rec} contact angles plotted in Fig. 3b as functions of droplet volume V for tilt angle α equal to $0^\circ, 12 \pm 1^\circ$, and $24 \pm 1^\circ$. As droplet volume and tilt angle increased, gravity caused the shape of the droplet to be asymmetrical and the receding contact angle θ_{rec} decreased. The measured advancing θ_{adv} and receding θ_{rec} contact angles were used in the *Surface Evolver* model to predict the shape of pendant droplets on tilted surfaces. Fig. 3c shows the resulting simulated droplet profile for droplet volume $V = 50 \mu\text{L}$ and tilt angle $\alpha = 24^\circ$. Comparing Figs. 3a and 3c shows good agreement between the experimental and simulated droplet profiles. As such, the *Surface Evolver* model was considered to be also valid for tilted windows and was used to predict the shape of large pendant droplets on tilted surfaces.

Fig. 3d plots the predicted maximum attainable droplet volume V_{max} corresponding to the maximum volume before the droplet detached from a horizontal surface as a function of droplet contact angle θ_c . On well-wetting surfaces with low droplet contact angle, adhesive forces between the water and the surface dominated and the surface was able to support droplets with large maximum volume V_{max} around $300 \mu\text{L}$. As the contact angle increased, the adhesive forces between the droplet and the surface decreased and the maximum droplet volume V_{max} approached $0 \mu\text{L}$ for $\theta_c \geq 140^\circ$.

4.2. Effect of droplet arrangement and size distribution

To investigate the impact of droplet spatial arrangement on the normal-hemispherical transmittance T_{nh} of horizontal windows, monodisperse pendant droplets were arranged either randomly or in an ordered hexagonal pattern. Similarly, to investigate the impact of the droplet size distribution, monodisperse or polydisperse

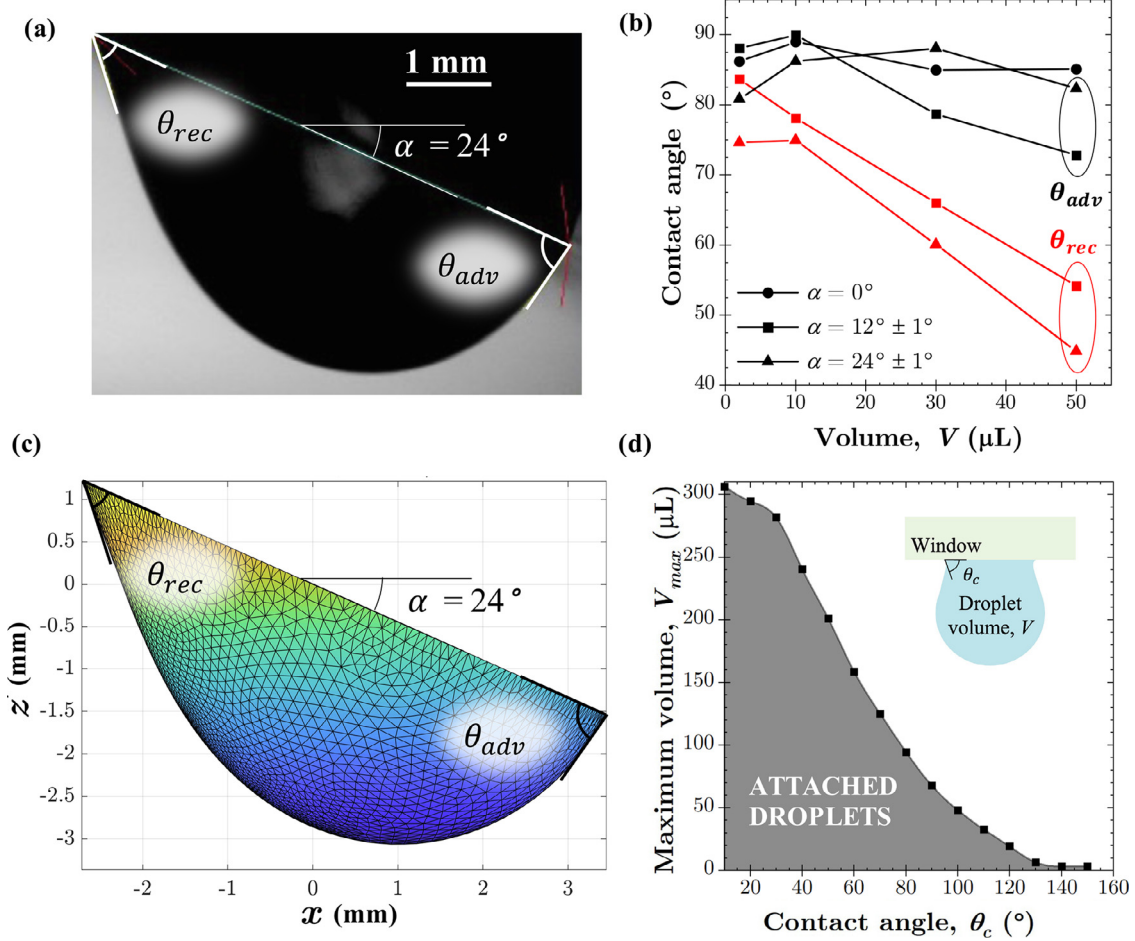


Fig. 3. (a) Photograph of a droplet of volume $V = 50 \mu\text{L}$ on a PVC slab with tilt angle $\alpha = 24^\circ$. (b) Measured receding θ_{rec} and advancing θ_{adv} contact angles as a function of droplet volume V for tilt angle α equal to 0° , $12 \pm 1^\circ$, and $24 \pm 1^\circ$. (c) Simulation of the tilted pendant droplet shape with volume $V = 50 \mu\text{L}$ and tilt angle $\alpha = 24^\circ$. (d) Maximum volume V_{max} before the pendant water droplet detaches from a horizontal window predicted as a function of contact angle θ_c .

droplets with a normal size distribution were simulated with a random spatial arrangement. For polydisperse droplets with mean volume \bar{V} , two normal droplet size distributions were simulated with standard deviation σ equal to $0.15\bar{V}$ or $0.3\bar{V}$. The droplet volume ranged from $0.1\bar{V}$ to $2\bar{V}$ and was discretized in increments of $0.1\bar{V}$. Table 1 summarizes the predicted normal-hemispherical transmittance T_{nh} of horizontal windows with droplet surface area coverage $f_A = 50\%$, droplet mean volume $\bar{V} = 25 \mu\text{L}$ or $75 \mu\text{L}$, and contact angle $\theta_c = 60^\circ$ or 90° . It establishes that, for a given contact angle θ_c and mean droplet volume \bar{V} , the spatial arrangement of non-cap shaped droplets had a negligible effect on the window's normal-hemispherical transmittance. The same conclusions were previously obtained for non-absorbing cap-shaped droplets pendant from horizontal windows [7]. However, Table 1 indicates that the mean volume \bar{V} had an important impact on the trans-

mittance of windows for large droplets, unlike in the case of cap-shaped droplets [3–5,7,10,16]. Despite the dependence of transmittance on the mean volume \bar{V} , the impact of the droplet size distribution was found to be negligible for relatively narrow size distributions.

4.3. Effect of droplet volume

Fig. 4a plots the predicted normal-hemispherical transmittance T_{nh} as a function of the droplet volume V for large droplets pendant from a horizontal window with contact angle θ_c equal to 30° , 60° , and 90° and surface area coverage $f_A = 50\%$. Droplets were monodisperse and arranged in a hexagonal pattern. Note that the same results are expected for non-absorbing polydisperse and/or randomly distributed droplets with the same mean volume \bar{V} and

Table 1

Normal-hemispherical transmittance of horizontal windows supporting large droplets with contact angle θ_c of 60° or 90° , ordered or random spatial arrangements, and monodisperse or polydisperse with a normal size distribution. Simulations were performed for a window surface area of 400 cm^2 with projected surface area coverage $f_A = 50\%$.

Spatial arrangement	Size distribution	Standard deviation σ (μL)	T_{nh}		
			$\bar{V} = 75 \mu\text{L}$ $\theta_c = 60^\circ$	$\bar{V} = 25 \mu\text{L}$ $\theta_c = 60^\circ$	$\bar{V} = 25 \mu\text{L}$ $\theta_c = 90^\circ$
Hexagonal	Monodisperse	-	0.825	0.789	0.700
Random	Monodisperse	-	0.836	0.795	0.700
Random	Polydisperse	$0.15\bar{V}$	0.834	0.797	0.702
Random	Polydisperse	$0.30\bar{V}$	0.832	0.801	0.702

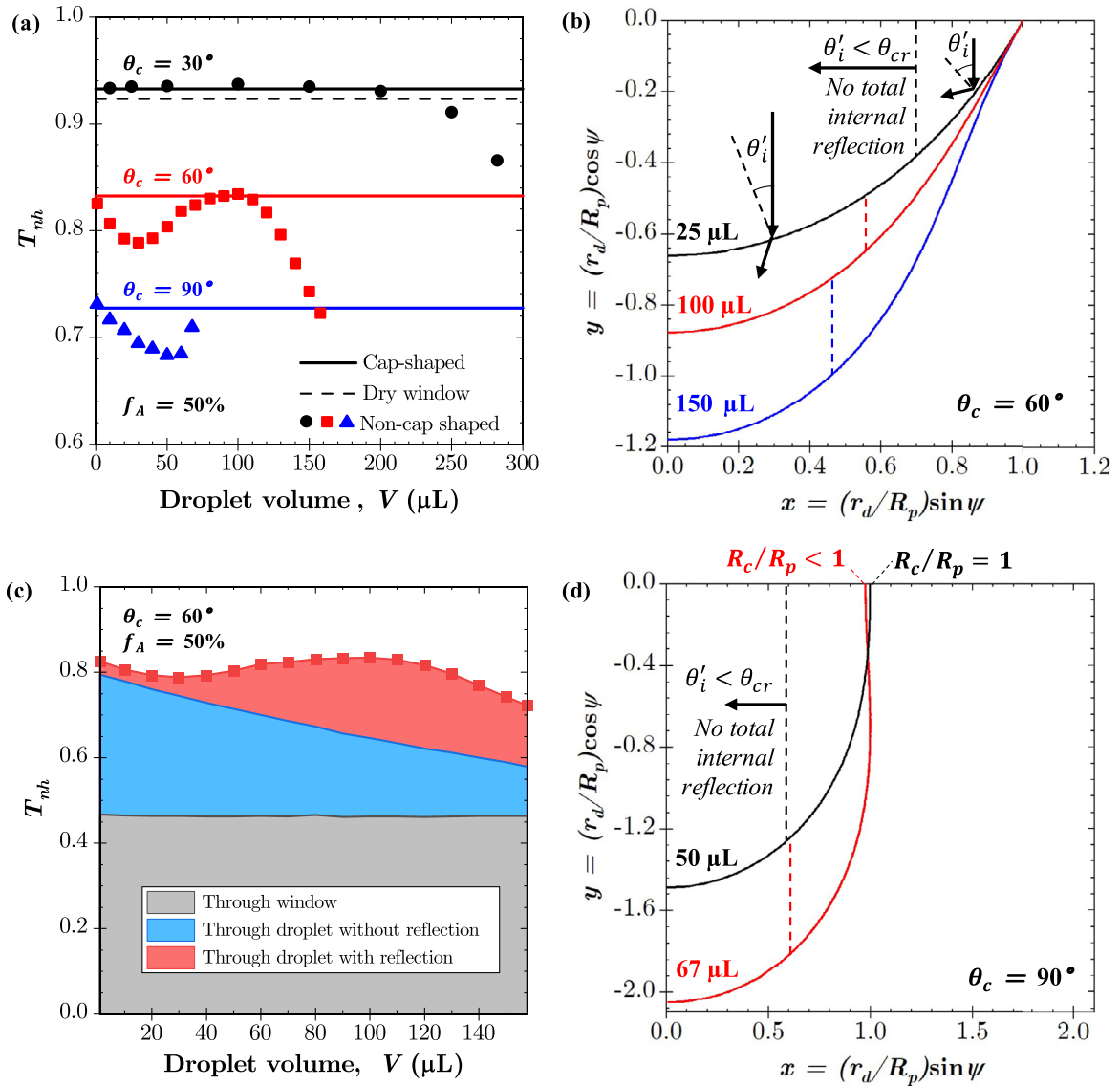


Fig. 4. (a) Normal-hemispherical transmittance T_{nh} of a horizontal window with cap-shaped and large droplets as a function of droplet volume V for contact angle $\theta_c = 30^\circ, 60^\circ,$ and 90° . (b) Normalized droplet contours for droplet volume $V = 25 \mu\text{L}, 100 \mu\text{L},$ and $150 \mu\text{L}$ and contact angle $\theta_c = 60^\circ$. (c) Transmittance as a function of droplet volume showing the fraction of photons transmitted through the window and transmitted through the droplets with and without reflection events. (d) Normalized droplet contours for $V = 50 \mu\text{L}$ and $67 \mu\text{L}$ with contact angle $\theta_c = 90^\circ$.

contact angle θ_c , as previously demonstrated. Droplet volume V ranged from $1 \mu\text{L}$ to V_{\max} (see Fig. 3d). The transmittances of a dry glass window and of a window supporting cap-shaped droplets with the same contact angle θ_c and surface area coverage f_A are also plotted as references. The predicted normal-hemispherical transmittance T_{nh} of windows supporting large droplets was nearly identical to that supporting cap-shaped droplets for (a) droplet volume $V < 200 \mu\text{L}$ and contact angle $\theta_c = 30^\circ$ and for (b) $V < 10 \mu\text{L}$ and contact angle $\theta_c = 60^\circ$ and 90° . Beyond these droplet volumes, the transmittance T_{nh} was found to be up to 13% smaller for large non-cap shaped droplets than for cap-shaped droplets. This was due to distortions in the droplet shape caused by gravity. These distortions caused the incidence angle θ'_i at the droplet/air interface to exceed the droplet contact angle in certain areas. Such an increase in the angle of incidence θ'_i increased the number of photons undergoing total internal reflection at the droplet/air interface and decreased the normal-hemispherical transmittance T_{nh} . Therefore, assuming large droplets to be cap-shaped generally caused the transmittance T_{nh} of horizontal windows to be overestimated.

However, it can provide an upper bound to the actual transmittance.

Fig. 4b shows the droplet contours for contact angle $\theta_c = 60^\circ$ and droplet volume V equal to $25 \mu\text{L}, 100 \mu\text{L},$ and $150 \mu\text{L}$. To compare the shapes of droplets of different volumes, the droplet contours $r_d(\psi, \phi)$ were normalized with respect to their projected radius R_p . The incidence angle θ'_i at the droplet/air interface is shown schematically for normal incidence. Fig. 4b illustrates that when the incidence angle θ'_i of a photon at the droplet/air interface was larger than the critical angle for total internal reflection, given by $\theta_{cr} = \sin^{-1}(n_a/n_w) = 48.6^\circ$, i.e., $\theta'_i > \theta_{cr}$, it was reflected back inside the droplet. Fig. 4c plots the fractions of rays that were (i) transmitted directly through the window, (ii) transmitted through the droplet without any reflection, and (iii) transmitted through the droplet with at least one reflection event as functions of droplet volume V for contact angle $\theta_c = 60^\circ$ and $f_A = 50\%$. Fig. 4b indicates that the fraction of the droplet/air interface such that $\theta'_i < \theta_{cr}$ decreased as the droplet volume V increased. This observation explained the decrease in the fraction of photons

transmitted through the droplet without reflection with increasing droplet volume observed in Fig. 4c. The same phenomenon was observed for contact angle θ_c of 30° and 90° and caused the transmittance T_{nh} to decrease with increasing droplet volume V , as observed in Fig. 4a. For contact angle $\theta_c = 60^\circ$, the fraction of photons transmitted through the droplet that experienced at least one reflection event increased as droplet volume V increased. Thus, despite a larger fraction of photons undergoing total internal reflection at the droplet/air interface, the droplet shape was such that these photons were eventually transmitted through the droplet. This phenomenon resulted in a maximum in the normal-hemispherical transmittance T_{nh} observed in Fig. 4a for $\theta_c = 60^\circ$ at $V = 100 \mu\text{L}$. For volume $V > 100 \mu\text{L}$, T_{nh} decreased with increasing volume due to a decrease in the fraction of photons transmitted with and without reflection.

Fig. 4d shows the normalized droplet contours for contact angle $\theta_c = 90^\circ$ and droplet volume $V = 50 \mu\text{L}$ and $V_{\text{max}} = 67 \mu\text{L}$. Two main differences between the droplet contours at $V = 50 \mu\text{L}$ and $67 \mu\text{L}$ were responsible for the corresponding increase in T_{nh} observed in Fig. 4a. First, the droplet with $V_{\text{max}} = 67 \mu\text{L}$ had a slightly larger fraction of its droplet/air interface such that $\theta'_i < \theta_{cr}$ compared to the droplet with $V = 50 \mu\text{L}$. As previously discussed, this tends to increase transmittance. Second, Fig. 4d shows a slight bulge in the droplet contour at $V_{\text{max}} = 67 \mu\text{L}$ that was not present at $V = 50 \mu\text{L}$. This caused the droplet projected radius R_p to exceed the droplet contact circle radius R_c , i.e., $R_c/R_p < 1$ unlike for droplet volume $V = 50 \mu\text{L}$ where $R_c/R_p = 1$. Thus, for a given surface area coverage f_A (defined based on R_p), the fraction of the window in contact with droplets was equal to f_A for droplet volume $V = 50 \mu\text{L}$ but it was less than f_A for droplet volume $V_{\text{max}} = 67 \mu\text{L}$. As a result, a smaller fraction of photons passed through the window/droplet contact surface and were then back-scattered at the droplet/air interface. This caused a corresponding increase in transmittance for droplet volume $V_{\text{max}} = 67 \mu\text{L}$ and contact angle $\theta_c = 90^\circ$ (Fig. 4a).

4.4. Effect of droplet contact angle

Fig. 5a plots the normal-hemispherical transmittance T_{nh} of a horizontal window supporting large droplets as a function of contact angle θ_c for monodisperse droplets of volume V equal to $10 \mu\text{L}$, $25 \mu\text{L}$, and $50 \mu\text{L}$ and surface area coverage $f_A = 50\%$. Fig. 5a also shows the transmittances of a dry glass window and of a window supporting cap-shaped droplets with the same contact angle θ_c and surface area coverage f_A . Note that T_{nh} was independent of droplet volume V for cap-shaped droplets [3,7,10]. For contact angle $\theta_c \leq \theta_{cr}$, the normal-hemispherical transmittances T_{nh} of a window supporting cap-shaped or non-cap shaped droplets were nearly identical, independent of contact angle θ_c , and slightly larger than that of dry glass. However, for contact angles $\theta_c > \theta_{cr}$ the normal-hemispherical transmittance decreased sharply and even more so for large droplets. This was caused by an increase in total internal reflection of photons at the droplet/air interface when $\theta_c > \theta_{cr}$. It was also observed in previous studies on cap-shaped droplets [3,7,13]. The minimum normal-hemispherical transmittance T_{nh} occurred around $\theta_c = 90^\circ$ for droplet volume $V \leq 25 \mu\text{L}$ and cap-shaped droplets [3,7,13] and around $\theta_c = 80^\circ$ for $V = 50 \mu\text{L}$. As contact angle θ_c increased further, T_{nh} increased as fewer photons were internally reflected at the droplet/air interface, as discussed in previous studies [3,7,13]. Overall, these results indicate that assuming large droplets to be cap-shaped causes the window transmittance T_{nh} to be overestimated for $\theta_{cr} \leq \theta_c \leq 90^\circ$. They also suggest that hydrophilic windows with droplet contact angle $\theta_c < \theta_{cr}$ are preferable to maintain high window transmittance T_{nh} for both large droplets and small cap-shaped droplets.

Fig. 5a indicates that transmittance decreased with increasing volume V for contact angle $\theta_c < 100^\circ$. However, it slightly in-

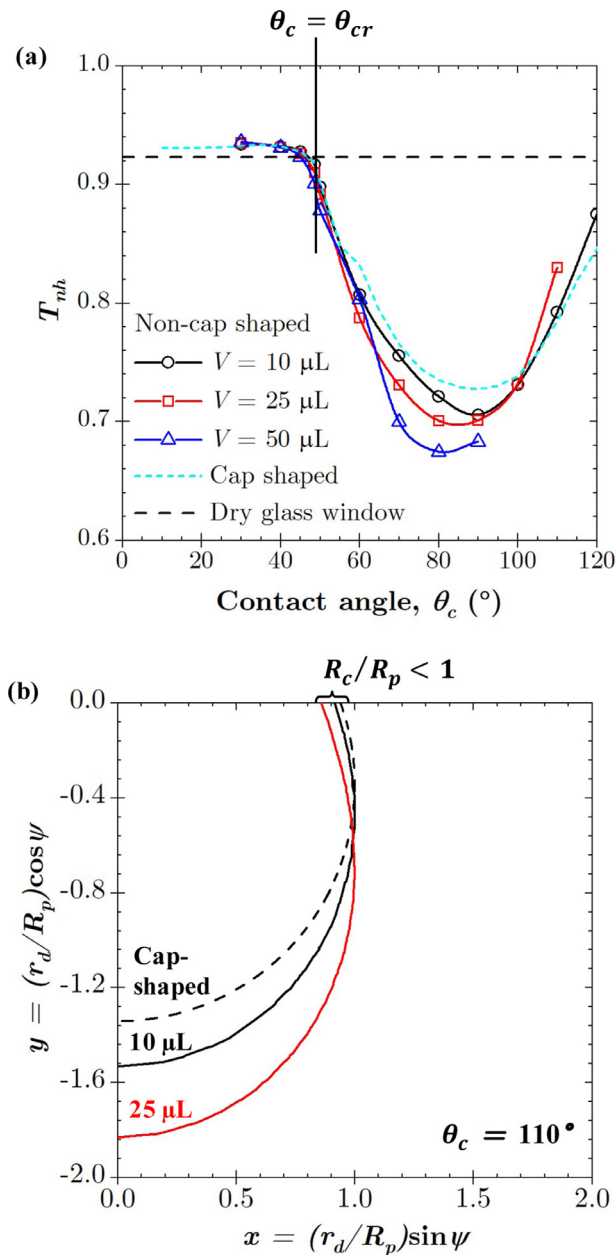


Fig. 5. (a) Normal-hemispherical transmittance T_{nh} of a horizontal window with surface area coverage $f_A = 50\%$ supporting cap-shaped and non-cap shaped droplets as a function of contact angle θ_c for various droplet volumes V . (b) Normalized cap-shaped and non-cap shaped droplet contours for $10 \mu\text{L}$ and $25 \mu\text{L}$ with contact angle $\theta_c = 110^\circ$.

creased with increasing volume V for larger contact angles. Fig. 5b plots the droplet contours for a cap-shaped droplet and large droplets with volume V of $10 \mu\text{L}$ and $25 \mu\text{L}$ and contact angle of $\theta_c = 110^\circ$ normalized with respect to each droplet's projected radius $R_p = 1.41 \text{ mm}$ and 1.79 mm , respectively. Fig. 5b indicates that R_c/R_p decreased with increasing droplet volume V as gravity pulled the droplet away from the surface. This further reduced reflection at the droplet/air interface, as discussed previously. It also caused T_{nh} for large droplets to exceed that of cap-shaped droplets with the same contact angle $\theta_c > 100^\circ$, as observed in Fig. 5a.

4.5. Effect of window tilt angle

Fig. 6 plots the predicted normal-hemispherical transmittance T_{nh} as a function of droplet volume V for window tilt angle α equal

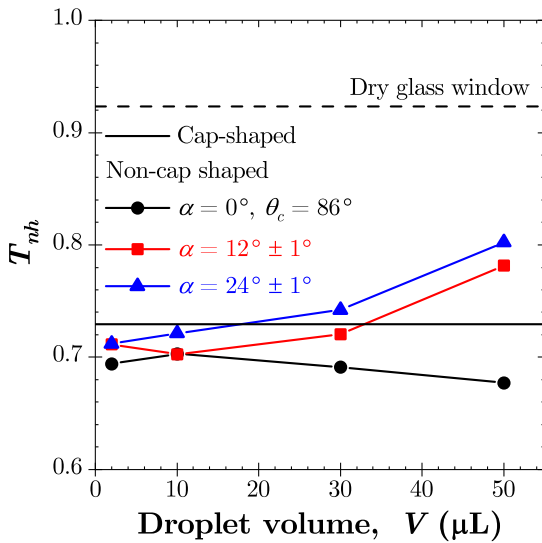


Fig. 6. Normal-hemispherical transmittance T_{nh} of a tilted window supporting pendant droplets with surface area coverage $f_A = 50\%$ as a function of droplet volume V for tilt angles α equal to 0° , $12 \pm 1^\circ$, and $24 \pm 1^\circ$.

to 0° , $12 \pm 1^\circ$, and $24 \pm 1^\circ$. It indicates that T_{nh} increased with increasing droplet volume V and/or window tilt angle $\alpha > 0^\circ$. This was caused by gravitational forces which caused the droplet receding contact angle θ_{rec} to decrease with increasing volume V and tilt

angle α (Fig. 3b). This increasingly asymmetric shape reduced total internal reflection particularly in the upper part of the droplet/air interface (see Fig. 3c). These results suggest that even a slight window tilt could be used to increase the normal-hemispherical transmittance of droplet-covered windows.

4.6. Effect of droplet surface area coverage

Figs. 7a–c plot the normal-hemispherical transmittance T_{nh} as a function of surface area coverage f_A for large pendant droplets on horizontal windows with various droplet volumes V and contact angles θ_c equal to (a) 30° , (b) 60° , and (c) 90° , respectively. Similarly, Figs. 7d–7f plot the normal-hemispherical transmittance T_{nh} as a function of surface area coverage f_A for pendant droplets of various volume V on a window with tilt angle α equal to (d) 0° , and (e) $12^\circ \pm 1^\circ$, and (f) $24^\circ \pm 1^\circ$, respectively. In each case, the transmittance T_{nh} of a window supporting cap-shaped droplets as a function of surface area coverage f_A is shown for the corresponding window tilt angle α and contact angle θ_c . For the horizontal window, θ_c was taken as 86° while for tilted surfaces the measured advancing θ_{adv} and receding θ_{rec} contact angles were reported in Fig. 3b as functions of the droplet volume V . As observed with cap-shaped droplets [7,8,13], the presence of large droplets caused the transmittance T_{nh} to decrease linearly with increasing surface area coverage f_A for both horizontal and tilted windows. Indeed, for contact angle $\theta_c = 90^\circ$, volume $V = 50 \mu\text{L}$, and surface coverage $f_A = 90\%$, the presence of large droplets reduced the window transmittance by 46% compared to a dry window.

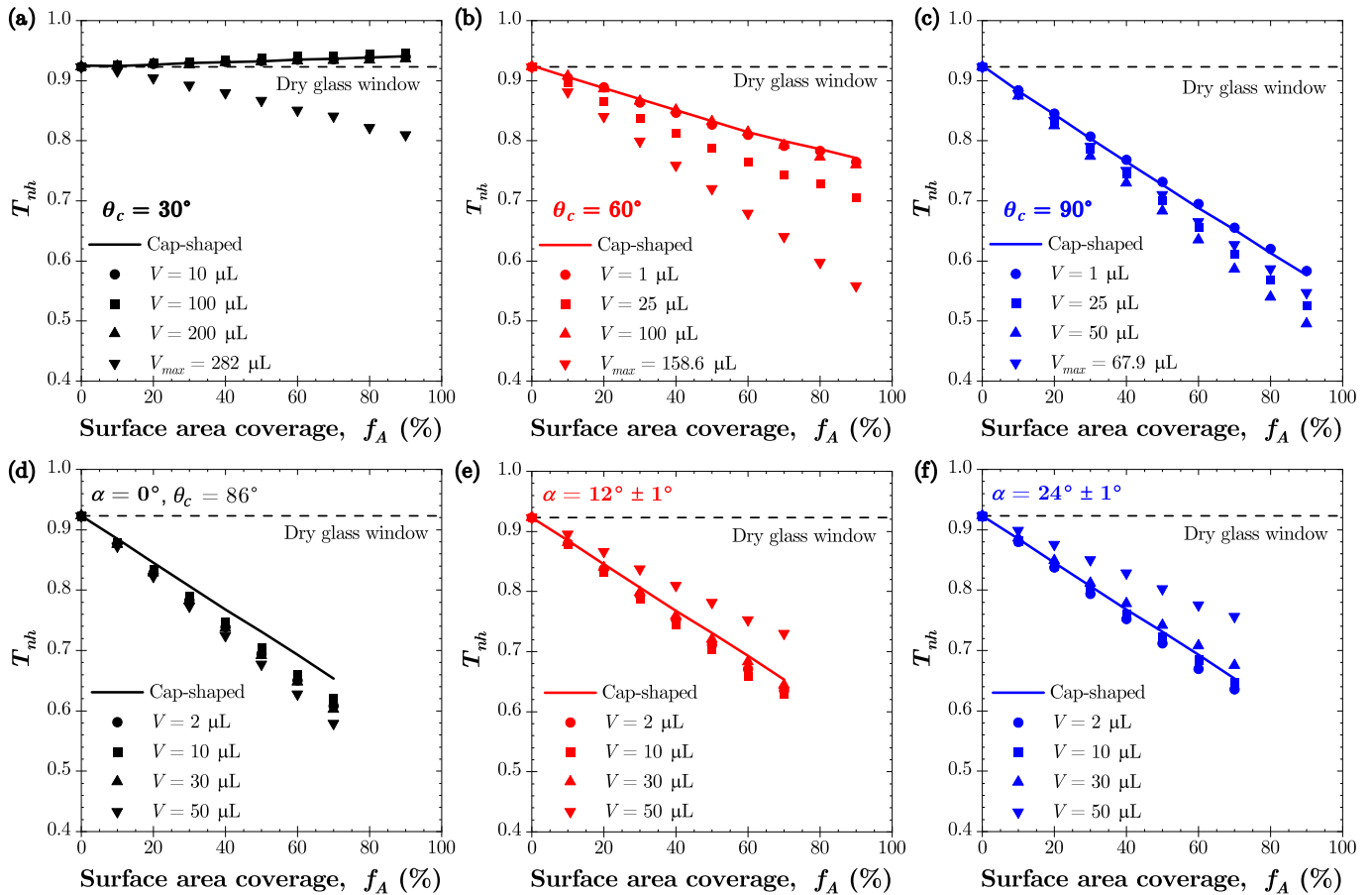


Fig. 7. Normal-hemispherical transmittance T_{nh} of a horizontal window supporting large pendant droplets of various volumes V as a function of surface area coverage f_A for contact angles θ_c equal to (a) 30° , (b) 60° , and (c) 90° . Normal-hemispherical transmittance T_{nh} of a tilted window supporting large pendant droplets with various volumes V as a function of surface area coverage f_A for tilt angle α equal to (d) 0° , (e) $12^\circ \pm 1^\circ$, and (f) $24^\circ \pm 1^\circ$. For tilt angle $\alpha = 0^\circ$, the droplet contact angle was taken as $\theta_c = 86^\circ$. For nonzero tilt angle α , droplet advancing θ_{adv} and receding θ_{rec} contact angles were given by Fig. 3b.

Figs. 7a–7c indicate that assuming droplets to be cap-shaped on a horizontal window caused T_{nh} to be overestimated. The discrepancy increased with increasing surface area coverage f_A and droplet volume V . Indeed, neglecting the gravity-induced deformation of large droplets caused the transmittance T_{nh} to be overestimated by a relative error as large as 37% for $\theta_c = 60^\circ$, $f_A = 90\%$, and $V = V_{max}$. On the other hand, Fig. 7e and 7f show that assuming large droplets to be cap-shaped on a tilted window caused T_{nh} to be underestimated by as much as 14% for droplet volume $V \geq 50 \mu\text{L}$ and surface area coverage $f_A = 70\%$. This was attributed to the asymmetrical shape of large droplets, as discussed previously. Note that, in practice, a tilted window tends to have a lower maximum droplet surface area coverage compared to a horizontal window since droplet run-off occurs more readily. As such, tilted windows may be preferable for minimizing the effects of droplets on the window transmittance.

4.7. Directional-hemispherical transmittance

Fig. 8a plots the directional-hemispherical transmittance T_{dh} as a function of the polar angle of incidence θ_i for a horizontal window with surface area coverage $f_A = 70\%$ supporting large pendant droplets of contact angle θ_c equal to 30° , 60° , and 90° and volume V equal to $282 \mu\text{L}$, $159 \mu\text{L}$, and $50 \mu\text{L}$, respectively. These droplet volumes V were selected since their normal-hemispherical transmittance T_{nh} differed the most from that of cap-shaped droplets (see Fig. 4a). Note that the directional-hemispherical transmittance T_{dh} was independent of the azimuthal angle of incidence γ_i due to the axisymmetric shape of droplets pendant from a horizontal surface. The directional-hemispherical transmittances T_{dh} for a dry glass window and for windows supporting cap-shaped droplets with the same contact angle θ_c and surface area coverage f_A are also shown as references. The directional-hemispherical transmittance T_{dh} of a dry window decreased with increasing polar incidence angle θ_i due to reflection at the air/window interface. Fig. 8a demonstrates that this was also the case for both cap-shaped and large droplets with contact angle $\theta_c = 30^\circ$ where reflection at the air/glass interface dominated and the directional-hemispherical transmittance T_{dh} decreased monotonically with increasing polar incidence angle θ_i . However, for large droplets with contact angles $\theta_c = 60^\circ$ and 90° as well as for cap-shaped droplets with contact angle $\theta_c = 90^\circ$ the directional-hemispherical transmittance T_{dh} increased with increasing polar incidence angle θ_i up to 50° due to decreasing reflection at the water/air interface [7,10]. Nonetheless, for $\theta_i > 50^\circ$, reflection at the front air/glass interface began to dominate and T_{dh} decreased following the trends observed in the transmittance T_{dh} of a dry window.

Fig. 8b plots the directional-hemispherical transmittance T_{dh} as a function of the polar angle of incidence θ_i for azimuthal angle of incidence γ_i equal to 0° and 180° for a window with tilt angle $\alpha = 24^\circ \pm 1^\circ$ and surface area coverage $f_A = 70\%$ supporting large droplets of volume $V = 50 \mu\text{L}$. The directional-hemispherical transmittances T_{dh} of a dry tilted window and a tilted window supporting cap-shaped droplets with contact angle $\theta_c = 86^\circ$ and surface area coverage $f_A = 70\%$ are also shown. Fig. 8b indicates that the directional-hemispherical transmittance T_{dh} of tilted windows supporting large droplets varied with the azimuthal angle of incidence γ_i , unlike for horizontal windows. This was due to the asymmetric shape of droplets on tilted windows and has also been observed in previous studies [15]. Furthermore, the directional-hemispherical transmittance T_{dh} of a tilted window covered with large non-cap shaped droplets was larger than that with cap-shaped droplets for both values of azimuthal angle of incidence γ_i and all values of polar angle of incidence θ_i . This suggests that tilted windows are preferable to horizon-

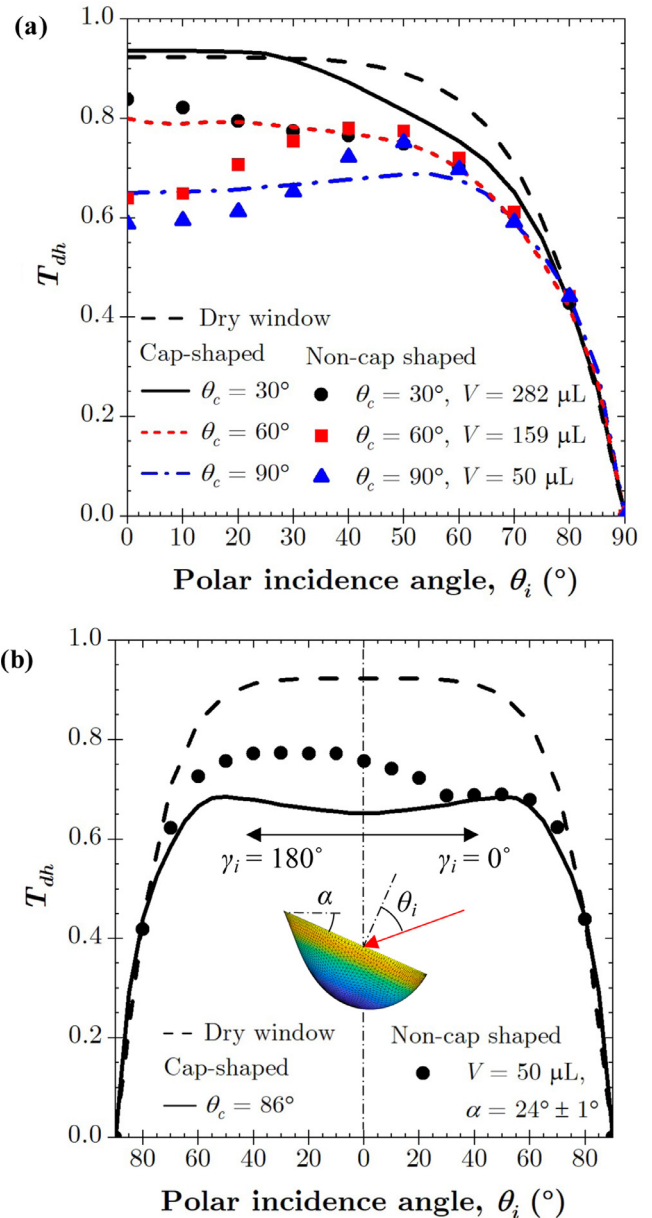


Fig. 8. (a) Directional-hemispherical transmittance T_{dh} of a horizontal window supporting cap-shaped and large pendant droplets as a function of the polar incidence angle θ_i for contact angle θ_c equal to 30° , 60° , and 90° and droplet volumes V equal to $282 \mu\text{L}$, $159 \mu\text{L}$, and $50 \mu\text{L}$, respectively, and (b) directional-hemispherical transmittance T_{dh} of a window with tilt angle $\alpha = 24^\circ \pm 1^\circ$ supporting cap-shaped and large pendant droplets with volume $V = 50 \mu\text{L}$ as a function of the polar angle of incidence θ_i for azimuthal angle of incidence γ_i equal to 0° and 180° . For both horizontal and tilted windows the droplet surface area coverage f_A was equal to 70%.

tal windows for maintaining high window transmittance when droplets are present regardless of the direction of the incident radiation.

5. Conclusion

This study established that the normal-hemispherical transmittance T_{nh} and the directional-hemispherical transmittances T_{dh} of horizontal and tilted transparent windows supporting large pendant and non-absorbing droplets may depend strongly and in a non-trivial way on the droplet volume, contact angle, surface area coverage, and window tilt angle. First, the shape of large pendant water droplets was simulated accounting for gravitational and

surface tension forces using the *Surface Evolver* program. Then, the normal-hemispherical and directional-hemispherical transmittances of a window supporting the simulated non-absorbing droplets was predicted using the Monte Carlo ray-tracing method. The droplet spatial arrangement on the window had no effect on the transmittance. The predicted transmittance was the same for monodisperse droplets and polydisperse droplets with the same mean volume and a relatively narrow size distribution. For small droplet volumes $V < 10 \mu\text{L}$ and/or contact angles $\theta_c < \theta_{cr}$ the droplets could be treated as cap-shaped for predicting the transmittance. However, for larger volumes $V \geq 10 \mu\text{L}$ and/or contact angles $\theta_c \geq \theta_{cr}$, the transmittance T_{nh} of a horizontal window was smaller when supporting large droplets than when supporting cap-shaped droplets of equal contact angle by up to 27%. This was due to gravity-induced deformations in the droplet shape which increased the photon's incidence angle at the droplet/air interface and thus increased total internal reflection. In most cases, the transmittance T_{nh} of horizontal windows decreased with increasing droplet volume and contact angle. Conversely, droplets supported by tilted windows featured an asymmetrical shape that reduced total internal reflection and increased transmittance with increasing droplet volume and window tilt angle. The normal-hemispherical transmittance T_{nh} decreased linearly with increasing droplet surface area coverage for both horizontal and tilted windows. Based on the present results, windows made of hydrophilic materials and/or with a tilt are preferable for maintaining high window transmittance in situations where droplets tend to be large.

Declaration of Competing Interest

The authors have no competing interest to declare.

CRedit authorship contribution statement

Jack Hoeniges: Conceptualization, Methodology, Software, Validation, Formal analysis, Investigation, Data curation, Writing – original draft, Visualization, Project administration. **Keyong Zhu:** Methodology, Software, Validation, Formal analysis, Investigation, Resources, Data curation. **William Welch:** Software, Investigation, Data curation. **Eylul Simsek:** Resources. **Laurent Pilon:** Conceptualization, Writing – review & editing, Supervision, Project administration, Funding acquisition.

Acknowledgment

This research was supported in part by the National Science Foundation NRT-INFEWS: Integrated Urban Solutions for Food, En-

ergy, and Water Management (Grant No. DGE-1735325). The authors would also like to thank Professor Gaurav Bhutani of the Indian Institute of Technology, Mandi for their assistance with the *Surface Evolver* program.

References

- [1] Mangi KH, Larbi Z, Legrand J, Pruvost J, Si-Ahmed EK. Passive thermal regulation approach for algofilm® photobioreactor through phase change. *Chem Eng Res Des* 2021;168:411–25.
- [2] Hoeniges J, Zhu K, Pruvost J, Legrand J, Pilon L. Impact of dropwise condensation on the biomass production rate in covered raceway ponds. *Energies* 2021;14(268).
- [3] Briscoe BJ, Galvin KP. The effect of surface fog on the transmittance of light. *Sol Energy* 1991;46(4):191–7.
- [4] Pollet IV, Pieters JG. Condensation and radiation transmittance of greenhouse cladding materials, Part 1: laboratory measuring unit and performance. *J Agric Eng Res* 1999;74(4):369–77.
- [5] Pollet IV, Pieters JG. Condensation and radiation transmittance of greenhouse cladding materials, Part 3: results for glass plates and plastic films. *J Agric Eng Res* 2000;77(4):419–28.
- [6] Pollet IV, Pieters JG, Deltour J, Verschoore R. Diffusion of radiation transmitted through dry and condensate covered transmitting materials. *Sol Energy Mater Sol Cells* 2005;86(2):177–96.
- [7] Zhu K, Pilon L. Transmittance of semitransparent windows with non-absorbing cap-shaped droplets condensed on their backside. *J Quant Spectrosc Radiat Transf* 2017;194:98–107.
- [8] Zhu K, Pilon L. Transmittance of semitransparent windows with absorbing cap-shaped droplets condensed on their backside. *J Quant Spectrosc Radiat Transf* 2017;201:53–63.
- [9] Bhardwaj R, Kortenaar MVt, Mudde RF. Influence of condensation surface on solar distillation. *Desalination* 2013;326:37–45.
- [10] Pieters JG, Deltour JM, Debruyckere MJ. Light transmission through condensation on glass and polyethylene. *Agric For Meteorol* 1997;85(1–2):51–62.
- [11] Zhu K, Li S, Pilon L. Light transfer through windows with external condensation. *J Quant Spectrosc Radiat Transf* 2018;208:164–71.
- [12] Huang Y, Feng C, Hoeniges J, Zhu K, Pilon L. Bidirectional transmittance of transparent windows with external or backside condensation of nonabsorbing cap-shaped droplets. *J Quant Spectrosc Radiat Transf* 2020;251:107039.
- [13] Tow EW. The antireflective potential of dropwise condensation. *J Opt Soc Am A* 2014;31(3):493–9.
- [14] De Gennes PG, Brochard-Wyart F, Quéré D. Capillarity and wetting phenomena: drops, bubbles, pearls, waves. New York, NY: Springer Science & Business Media; 2013.
- [15] Pieters JG, Deltour JM, Debruyckere MJ. Experimental determination of the geometry of real drops on transparent materials. *J Phys III* 1996;6(7):975–89.
- [16] Pollet IV, Pieters JG. Condensation and radiation transmittance of greenhouse cladding materials, Part 2: results for a complete condensation cycle. *J Agric Eng Res* 2000;75(1):65–72.
- [17] Simsek E, Zhu K, Kashanchi GN, Williams MJ, Galy T, Marszewski M, et al. Light transfer through semi-transparent glass panes supporting pendant droplets. *J Quant Spectrosc Radiat Transf* 2021;261:107493.
- [18] Brakke KA. The surface evolver. *Exp Math* 1992;1(2):141–65.
- [19] Bhutani G, Muralidhar K, Khandekar S. Determination of apparent contact angle and shape of a static pendant drop on a physically textured inclined surface. *Interfacial Phenom Heat Transf* 2013;1(1):29–49.
- [20] Sherbini AIE, Jacobi AM. Liquid drops on vertical and inclined surfaces: I. An experimental study of drop geometry. *J Colloid Interface Sci* 2004;273(2):556–65.